SCIENCE CHINA
Physics, Mechanics & Astronomy

· **Research Paper** ·

January 2010 Vol. 53 No.1: 187–192
doi: 10.1007/s11433-010-0076-3

Simulation of interplanetary scintillation with SSSF and SSDF mode

LIU LiJia & PENG Bo*

National Astronomical Observatories, Chinese Academy of Sciences, Beijing 100012, China

Received January 6, 2009; accepted May 5, 2009

The sun has the biggest effect on the Earth in many ways. Observing the solar wind is an important method to study the solar-earth environment. Ground-based interplanetary scintillation observations are an effective method of monitoring solar wind speed, studying the random fluctuations of the interplanetary plasma and the structures of radio sources. Two modes of single-station observations, namely, single station-single frequency (SSSF) and single station dual-frequency (SSDF), are briefly introduced and numerically simulated in this paper. The SSSF mode are easier to carry out and has been widely used. Although the observing system and data processing system of the SSDF mode are more complicated, it can measure the solar wind speed more accurately. A new SSDF system is under construction in Miyun, NAOC (the National Astronomical Observatories, Chinese Academy of Sciences), with a 50 m telescope, which will serve the Meridian Project, and this paper is devoted to preparing for this new system.

interplanetary scintillation, single station-single frequency, single station dual-frequency, simulation

The solar wind is the material in interplanetary space that comes from coronal expansion in the form of inhomogeneous plasma flow, which is the primary source of the interplanetary medium, and it connects the variations in the Sun with terrestrial physical phenomena. There are two ways to observe the solar wind: spacecraft measurement and ground-based measurement. The spacecraft method has one limitation, as it can only travel near the ecliptic plane and sample from a stable orbit, while the solar wind phenomenon is very stochastic [1]. Radiation from a distant compact radio source is scattered by the density irregularities in the solar wind plasma, which produces a random diffraction pattern on the ground. The motion of these irregularities converts this pattern into temporal intensity fluctuations which are observed as interplanetary scintillation (IPS). Ground-based IPS observations can measure the solar wind at any distance and also for a long period [2], which is also the main method to do research on the Sun-Earth system [3].

Since the discovery of IPS in 1964, many countries like Britain, India and Japan have begun to observe this phenomenon. China began IPS studies in the 1990s with the phased array mode of the Miyun Synthesis Radio Telescope (MSRT) at 232 MHz. Located at Miyun observatory in Beijing, it uses the Single-Station Single-Frequency (SSSF) mode [4]. Recently a new IPS observation system using the 50 m parabolic radio telescope, which is based on the Single-Station Dual-Frequency (SSDF) mode at S/X and UHF bands, is under construction to serve the National Meridian Project of China. The theory of IPS, SSSF mode and SSDF mode are discussed in sec. 1, sec. 2 describes the instrumentation for the Miyun 50 m telescope, sec. 3 gives simulated results for the two modes, and the discussion is presented in sec. 4.

1 Theory

1.1 The theory of IPS

Figure 1 shows the geometry of IPS. The z-axis is along the line-of-sight, and the x-axis is in the direction perpendicular to the z-axis pointing away from the Sun, with the y-axis

*Corresponding author (email: liulijiaredstar@yahoo.com.cn)

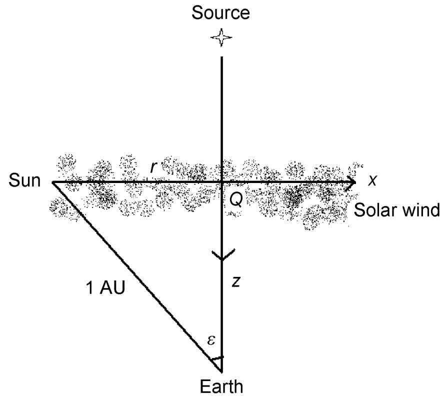

Figure 1 Geometry of the IPS concept.

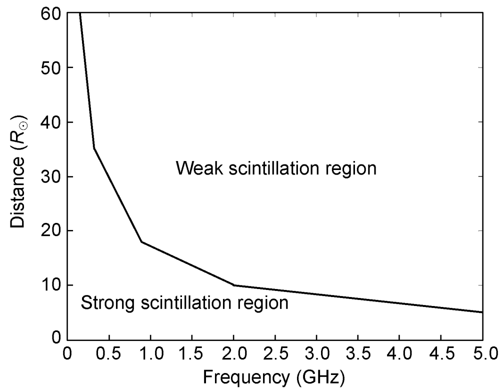

Figure 2 Frequency vs. distance for the weak and strong scintillation regions.

being normal to the paper. Q is the point closest to the Sun along the line-of-sight, and ε is the elongation angle, Sun-Earth-source. r is the distance between the Sun and Q. Z is the distance between Q and the Earth.

The degree of scintillation is characterized by the scintillation index m, which increases with decreasing distance r. The expression for m is shown below [5]:

$$m = \frac{\sqrt{\sigma_{\text{on}}^2 - \sigma_{\text{off}}^2}}{C_{\text{on}} - C_{\text{off}}}, \tag{1}$$

where C_{on} (C_{off}) is the average intensity of the on-source (off-source) signal, and σ_{on}^2 (σ_{off}^2) is the intensity-squared error of the on-source (off-source) signal. Here the on-source case refers to the telescope pointing at the radio source, and off-source the telescope pointing at the background sky away from the source. IPS is strongest in the region nearest the Sun, where we have the "strong scintillation region". In most of interplanetary space IPS is weak, which is called the "weak scintillation region". In the weak scintillation region $m \ll 1$. Previous studies show that the statistics of the scintillation are simply related to those of the turbulent interplanetary medium by a linear relationship, if the scintillation is weak [6, 7]. In the "strong scintillation region", however, the relationship is not straightforward, and the present study always deals with the weak scintillation case. The distance regime for the weak and strong regions is related to observing frequencies. Figure 2 shows the relationship between the frequency and distance regimes according to ref. [8]. Taking 327 MHz for example, when observing at this frequency, the regime for the strong and weak regions is: Putting the Sun at the center, within 35 $R_\odot$ is the strong scintillation region, and beyond is the weak scintillation region ($R_\odot$ is the radius of the Sun).

1.2 The theory of SSSF mode

SSSF refers to observing the IPS with a single station at a single frequency. There are two methods to obtain the solar wind speed from the SSSF mode by the observed spectra: the spectral multi-parameter model-fitting, and the characteristic frequencies methods. The former can measure the speed by adjusting the main parameters of the solar wind to fit the observed scintillation power spectra. The parameters are: α-power law index of the spatial spectrum of electron density, AR-axial ratio of solar wind irregularities, and V-solar wind speed. The latter can be determined by calculating two characteristic frequencies of the spectra: the Fresnel knee frequency f_{F} corresponding to Fresnel diffraction theory, and $f_{\min}$ the first minimum of the spectra. Then the solar wind speed can be calculated by either of the formulae shown below [1]:

$$V = f_{\text{F}}\sqrt{Z\pi\lambda}, \tag{2}$$

$$V = f_{\min}\sqrt{Z\lambda}, \tag{3}$$

where λ is the observing wavelength, and z is the distance between Q and the Earth.

1.3 The theory of SSDF mode

Being different from the SSSF mode, the SSDF mode adopts simultaneous dual-frequency observations to measure the solar wind speed, by deriving the first zero point of the normalized cross-spectrum (NCS) at two different frequencies. The expression is shown below [8, 9]:

$$V = Af_{\text{zero}}\sqrt{Z\lambda_1}, \tag{4}$$

where A is a correction factor which varies slightly with the solar wind parameters and is usually taken to be 1.1. In most cases, taking $A=1$ will cause no more than a 10 % error in the measured solar wind speed, which is acceptable [8, 9]. The two wavelengths are denoted by λ_1 and λ_2, where λ_1 is the larger one.

2 Introduction to the IPS observing system of the 50 m radio telescope

A new IPS observing system is under construction at the

Miyun station of NAOC near Beijing, China, for the 50 m radio telescope, adopting the SSDF mode to do the IPS observations. The characteristics of this telescope are shown in Table 1 [8, 10, 11] where R_s stands for the radius of the Sun. There are two groups of frequency bands for this telescope, S/X (2300/8400 MHz) and UHF (327/611MHz). Observing at different frequencies can measure the solar wind at different distances from the Sun, which is very important in researching the evolution of the solar wind. This observing system will be the only multi-band facility in China serving the Meridian Project.

The radio sources which have projected distances less than 0.5AU from the Sun, with flux densities equal to or greater than 2 Jy, and radio diameters less than 0.2″ will be selected to perform the observations. According to the characteristics of the 50 m radio telescope and the formula for IPS, simulations of SSSF and SSDF will be presented below. The adopted wavelength for the SSSF simulation is 92 cm, and for the SSDF it is 13/3.6 cm.

3 Simulation of SSSF and SSDF modes

3.1 Simulation of SSSF mode

In the weak scintillation region, the Born approximation is applicable. The interplanetary medium can be considered to be made up of many thin layers perpendicular to the line-of-sight. When the radio wave passes through these layers, only the phase of the radio wave changes, while its amplitude stays the same, which is referred as the "thin scintillation screen theory" [12–15]. In the weak scintillation region, the observed scintillation can be regarded as the sum of contributions from all these thin layers. For a layer of thickness d*Z*, the distance from the layer to the Earth is *Z*, and the spectra observed at the Earth should be [16]:

$$M_i(f,Z)\mathrm{d}Z=\left[\frac{2\pi f(\lambda r_e)^2}{V_x(Z)}\right]\times\int_{-\infty}^{\infty}\Phi_{\mathrm{ne}}(k_x,k_y,k_z=0,Z)F_{\mathrm{diff}}F_{\mathrm{source}}\mathrm{d}k_y\mathrm{d}Z, \quad (5)$$

where

$$F_{\mathrm{diff}}=4\sin^2\left[\frac{(k_x^2+k_y^2)\lambda Z}{4\pi}\right], \quad (6)$$

$$F_{\mathrm{source}}=\exp\left[-(k_x^2+k_y^2)Z^2\theta_0^2\right] \quad (7)$$

$$\Phi_{\mathrm{ne}}(k_x,k_y,k_z=0,Z)=Tr^{-4}\left[k_x^2+\left(\frac{k_y}{AR}\right)^2\right]^{-\alpha/2}. \quad (8)$$

Here Φ_{ne} is the electron density power spectrum at distance *Z*, *T* is a constant, F_{diff} and F_{source} are the Fresnel propagation filter parameter and the squared modulus of the radio source visibility. Because of $V_x(Z)$, the wave-number is related to the frequency $k_x=\frac{2\pi f}{V_x(Z)}$. We assume that the brightness of the radio source has a symmetrical-Gaussian distribution, i.e.

$$B(\theta)=\exp\left[\frac{-(\theta/\theta_0)^2}{2}\right],$$

Θ is the full width at half maximum of the source, so we have the angular diameter of the scintillating source $\theta_0=\Theta/2.35$ [7], for a certain radio source, where θ_0 is also known. The spectrum obtained from the Earth should be the sum of eq. (5).

$$M_i(f)=\int_0^{\infty}M_i(f,Z)\mathrm{d}Z. \quad (9)$$

One can see that $M_i(f)$ depends on the solar wind parameters: axis ratio AR, power law index α, and the solar wind speed *V*. So taking appropriate values to fit the observed spectra, one can obtain the parameters for the observational data. $\lambda=92$ cm is chosen for the simulations carried out below. Figures 3–5 present the examples of different parameters.

From Figure 3 one can see that the solar wind speed *V* mostly affects the Fresnel knee f_F and the first minimum of the spectra $f_{\min}$, which is in accord with formulas (2) and (3). Figures 4 and 5 present examples of different AR and α.

From Figures 4 and 5 one can see that AR mostly affects

Table 1 Characteristics of the 50 m radio telescope at Miyun, NAOC

Diameter	Efficiency (MHz)	Noise temperature (K)	Operating frequency (MHz)	Local frequency (KHz)	Channel bandwidth (MHz)	Integration interval (s)	T_{LNA} (K)
50	345/57.3%, 611/57%, 2500/59.9%, 7600/68.4%	⩽17	327, 611, 2300, 8400	Adjustable, less than 10 KHz	327/30, 611/60, 2300/360, 8400/1600	2, 20, 1, 2	⩽35
T_{sys} (K)	Receiver gain/dB	Receiver sensitivity	Area	Longest observing time (h)	Pointing precision (″)	IPS detecting area	IPS observing mode
⩽80	(150±1.5) dB	0.2 Jy (bandwidth 4 MHz, integration interval 2s, *S/N*=5	Orientation ±270°, pitching +5°–+90°	±6	19	⩾5R_s(S/X), ⩾25R_s(UHF)	SSSF, SSDF

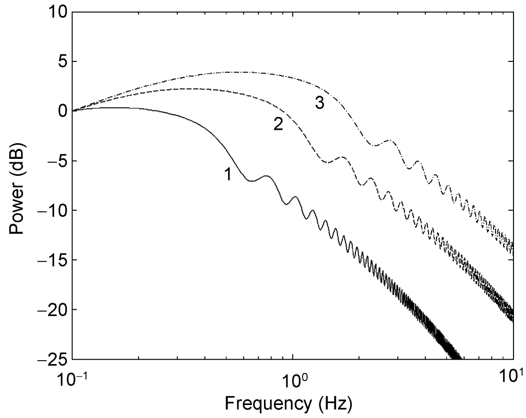

Figure 3 Simulated IPS spectra at various solar wind speeds V ($\lambda=92$ cm; $\alpha=3.5$; AR = 2; 1, $V=250$ km/s; 2, V=550 km/s; 3, $V=900$ km/s).

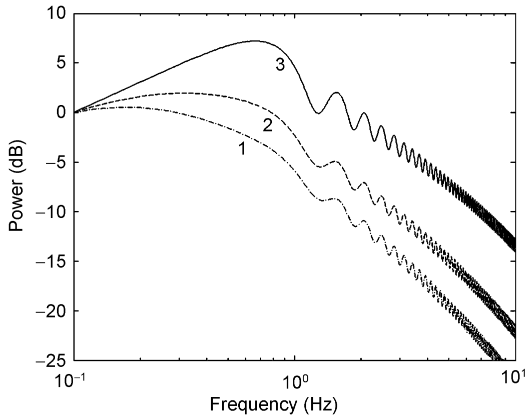

Figure 4 Simulated IPS spectra at various AR ($\lambda=92$ cm; $\alpha=3.5$; $V=$ 500 km/s; 1, AR = 1.0; 2, AR = 2.0; 3, AR = 3.0).

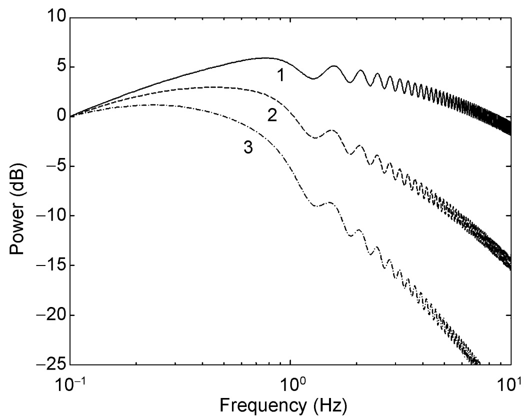

Figure 5 Simulated IPS spectra at various spectral indices α($\lambda=92$ cm; $V=500$ km/s; 1, $\alpha=2.0$; 2, $\alpha=3.0$; 3, $\alpha=4.0$).

the low frequency part of the power spectra, and the low frequency part becomes steeper when AR increases. However, the high frequency part changes slightly. α mostly affects the high frequency part of the spectra, and the high frequency part attenuates quickly when α increases, while the low frequency part does not obviously change.

According to the discussion shown above one can see that different parameters affect different parts of the spectrum. So, when carrying out the spectrum-fitting method, one can first choose the appropriate V and AR to fit the knee, and then choose α to fit the attenuation part.

A comparison of theoretical and numerical simulations was made (see Figure 6). The course of simulation is: first an inverse transformation of the theoretical values in the frequency domain is made to produce the data in the time domain, so called "observing data" S_1, which is without noise. White noise with amplitude between 0–1 is added to S_1 to form the simulated data S. Then S_1 and S will be processed in the same way to derive the IPS spectrum (see line 2 and line 3 in Figure 6). Because the theoretical data in the frequency domain only contain information on the amplitude without phase, the result will not be certain when carrying out the inverse transformation. Experiments were performed for several cases (for example the real part and imaginary part are equal, or the imaginary part is zero), from which one can conclude that the imaginary part has insignificant effect on the spectrum. Here we take the case, as an example, where the real part equals to the imaginary part.

It can be seen in Figure 6 that, from 0.1 to 0.12 Hz, the theoretical and numerical simulation results are different. But, within 0.12–5 Hz the three spectra tend to be almost the same. In Figure 6, line 1 is the theoretical spectrum, line 2 is the result from S_1, and line 3 is that from S. The parameters shown in Figure 6 are, AR=2, $\alpha=4$, $V=500$ km/s.

According to the experiments shown above one can see that the theoretical and numerical spectra are consistent. Due to some approximations made in the inverse transformation, a correction factor is required (of about 1.4) to make line 2 and line 3 conform to line 1 completely.

Figure 7 demonstrates, as an example, the comparison spectra for the four observing frequencies used at the 50 m

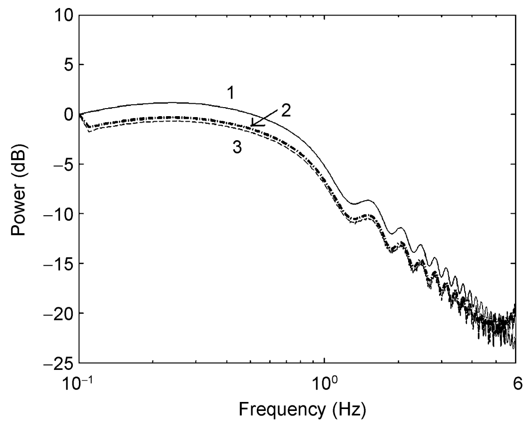

Figure 6 The simulated data and the computed spectrum for SSSF mode (1, theoretical spectrum; 2, spectrum without noise; 3, spectrum with noise; AR=2, α=4, $V=500$ km/s).

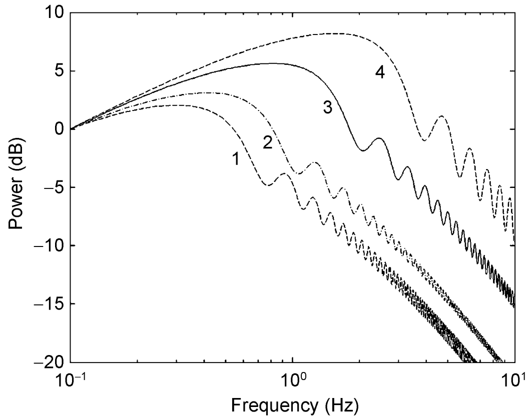

Figure 7 Spectra of four observation frequencies with the 50 m radio telescope in Miyun (1, 92 cm; 2, 49 cm; 3, 13 cm; 4, 3.6 cm; AR=1.5, α=3.5, V=500 km/s).

radio telescope in Miyun, where lines 1–4 are 92, 49, 13, and 3.6 cm, respectively. The parameters are: AR=1.5, α α=3.5, V=500 km/s. In Figure 7 one can observe that the spectrum falls off earlier at lower frequency. For the same signal to noise ratio, the spectrum observed at a lower frequency is more complete. Therefore a lower frequency will be preferable during IPS observations. The radio frequency interference environment at the telescope site should be taken into account in choosing an observing frequency before an observation.

3.2 Simulation of SSDF mode

The normalized cross-spectrum (NCS) of the SSDF mode is calculated by [3]

$$\mathrm{NCS}(f) = \frac{\mathrm{Re}(S_{12}(f))}{\sqrt{P_1(f)\cdot P_2(f)}}, \tag{10}$$

where

$$P_i(f) = C{r_e}^2\lambda_i^2 \int_0^\infty \frac{2\pi}{V} p(V)\mathrm{d}V \int_{-\infty}^{\infty} \mathrm{d}k_y \Phi_{ne}(k)\sin^2\left(\frac{k^2\lambda_i Z}{4\pi}\right) \times F_s(k)F_r(k),\ i=1,2, \tag{11}$$

$$S_{12}(f) = C{r_e}^2\lambda_1\lambda_2 \int_0^\infty p(V)\mathrm{d}V \int_{-\infty}^{\infty} \mathrm{d}k_y \Phi_{\mathrm{ne}}(k)\sin\left(\frac{k^2\lambda_1 Z}{4\pi}\right) \times \sin\left(\frac{k^2\lambda_2 Z}{4\pi}\right)\times F_s(k)F_r(k), \tag{12}$$

$$F_s = \exp[-(k_x^2+k_y^2)Z^2\theta_0^2], \tag{13}$$

$$F_r = \exp\left[\frac{-(k_x^2+k_y^2)}{(4\pi\cdot\Delta\lambda/\lambda^2 Z)^{-1/2}}\right], \tag{14}$$

where f is the temporal frequency, and S_{12} is the cross correlated spectrum at two frequencies f_1 and f_2. P_1 and P_2 are the power at each frequency. The corresponding wavelengths are λ_1 and λ_2, and $\lambda_1 > \lambda_2$. Sine functions express the Fresnel filters, and r_e=2.8×10^{-13} cm the electron radius,

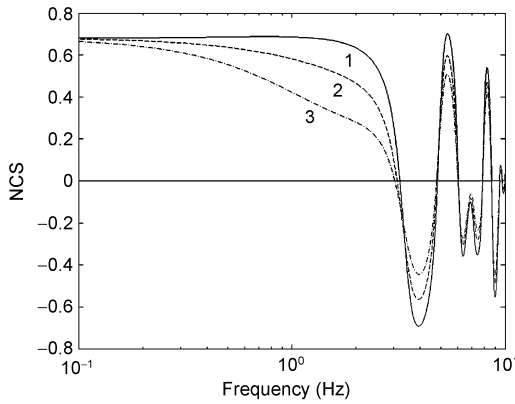

Figure 8 Simulated NCS at various AR (λ_1=13 cm, λ_1=3.6 cm; α=3.5; V=500 km/s; 1, AR=1.0; 2, AR=1.5; 3, AR=2.5).

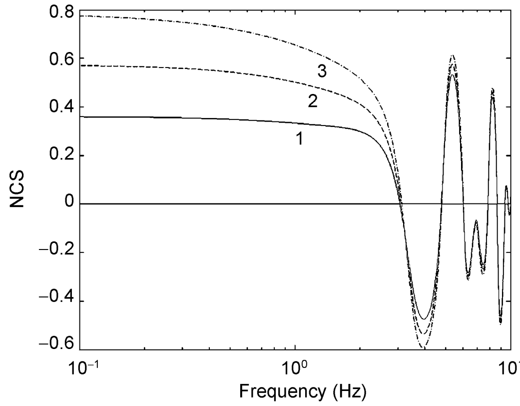

Figure 9 Simulated NCS at various α (λ_1=13 cm, λ_2=3.6 cm; AR=1.5; V=500 km/s; 1, α=2.0; 2, α=3.0; 3, α=4.0).

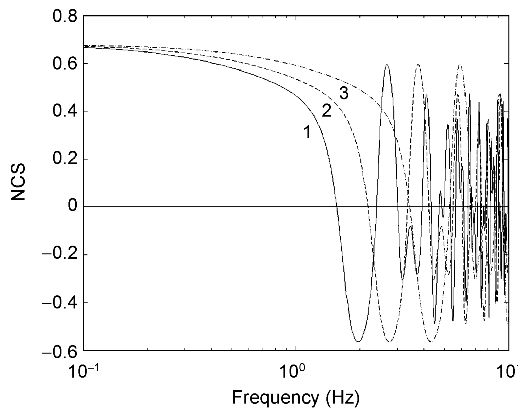

Figure 10 Simulated NCS at various solar wind speeds V (λ_1=13 cm, λ_2=3.6 cm; α=3.5; AR=1.5; 1, V=250 km/s; 2, V=350 km/s; 3, V=550 km/s).

$k = (k_x = 2\pi f / V,\ k_y, k_z = 0)$ is the three dimensional wavenumber, V is the velocity of the solar wind along the x axis, $P(V)$ is the distribution function of the solar wind speed, and Φ_{ne} is the spatial spectrum of the electron density at distance z. T and C are constants, and F_r and F_s are the filter parameter and the squared modulus of the radio source visibility. λ_1=13 cm and λ_2=3.6 cm are taken to consider how the parameters influence the power spectra in the SSDF mode.

One can conclude from Figures 8–10 that the different AR and α have little influence on the f_{zero} of the NCS, f_{zero} almost stays the same while these parameters change. But for different V, f_{zero} obviously changes, which is inosculated with formula (4).

4 Discussion

Among the two modes of ground-based single-station IPS observation, the SSSF observing instrument, data acquisition, and data reduction are more simple, and have been adopted by many observatories. For this mode, high signal to noise ratio (at least 25 dB [17]) data are needed. f_F can be calculated from almost every observation, because of the interactions of F_s and Φ_{ne}. During model-fitting, f_F can help us to find the appropriate solar wind speed. On the other hand, f_{min} does not always exist. Because of the effect of path integration, the minimums become flat, only the first minimum can be found, while the others are effaced. When AR increases, f_F becomes ambiguous, while f_{min} is easily affected by noise, AR and ε. The fitting accuracy is somehow affected by variations in solar wind parameters, and it is then hard to calculate the solar wind speed accurately [16].

With respect to the SSSF mode, the SSDF technique gives the solar wind speed via the first zero point of the cross correlation spectrum. And f_{zero} is apparently mostly affected by the velocity of the solar wind rather than other parameters. It has the advantages of higher accuracy for measuring solar wind speed and higher stability against wide variations in solar wind parameters. But it asks for more complexity in the observing instrument and data taking system, so it is not used as widely as the SSSF mode. The new system that is under construction at the Miyun station of the NAOC, China, with the 50m radio telescope, is adopting the SSDF mode to carry out IPS observations.

Supported by the Meridian Project of China (Grant No. [2006]2176)

1 Ma G Y. Reach and application of IPS. PHD Thesis. Beijing: Beijing Astronomical Observation, 1993. 1–3
2 Hewish A, Symonds M D. Radio investigation of the solar plasma. Planetary Space Sci, 1969, 17: 313
3 Scott L, Rickett B J, Armstrong J W. The velocity and the density spectrum of the solar wind from simultaneous three-frequency IPS observations. Astron Astrophys, 1983, 123: 191–206
4 Wu J H, Zhang X Z, Zheng Y J. IPS Observations at Miyun Station, BAO. Astrophys Space Sci, 2001, 278: 189–192; Cohen M H, Gundermann E J, Hardebeck H E, et al. Astrophys J, 1997, 147: 449C
5 Cohen M H, Gundermann E J, Hardebeck H E, et al. Interplanetary Scintillations. II Observations. Astrophys J, 1967, 147: 449C
6 Coles W A, Harmon J K, Lazarus A J, et al. Comparison of 74-MHz interplanetary scintillation and IMP 7 observations of the solar wind during 1973. J Geophys Res, 1978, 83: 3337–3341
7 Manoharan P K, Ananthakrishnan S. Determination of solar-wind velocities using single-station measurements of interplanetary scintillation. Roy Astron Soc, 1990, 244: 691–695
8 Zhang X Z. A study on the technique of observing interplanetary scintillation with simultaneous dual-frequency measurements. Chin J Astron Astrophys, 2007, 7: 712–720; Tokumaru M, Kondo T, Mori H, et al. J Geomagn Geoelectr, 1994, 46: 835–849
9 Tokumaru M, Kondo T, Mori H, et al. Solar wind motion near the sun derived from simultaneous interplanetary scintillation observations at 2 GHz and 8 GHz. J Geomagn Geoelectr, 1994, 46: 835–849
10 Wu J H, Zhang X Z. Ground-based monitoring technique of interplanetary disturbance. A report of national defense in China, 2003
11 Zhang X Z, Zhu X Y, Kong D Q, et al. Measurement of electronic properties of the Miyun 50 m Radio Telescope. Res Astron Astrophys, 2009, 3: 367–376; Yeh K C, Liu C H. Proc IEEE, 1982, 70: 324–360
12 Ishimara A. Radio wave scintillations in the ionosphere. IEEE, 1982, 70: 324–360
13 Ishimara A. Wave Propagation and Scattering in Random Media. New York: Academic, 1978
14 Salpeter E E. Scintillations due to a concentrated layer with a power-law turbulence spectrum. Radio Sci, 1975, 10: 107–114
15 SalpeterE E .Interplanetary scintillations I. Theory. Astrophys J, 1967, 147: 433–448
16 Ye P Z, Qiu Y H. Single station interplanetary scintillation measurement to diagnose solar wind velocity. Chin J Astron Astrophys, 1996, 16: 389–394
17 Tokumaru M T, Mori H, Tanaka T, et al. Solar wind velocity near the Sun: Results from interplanetary scintillation observations in 1989–1992. J Geomagn Geoelectr, 1994, 6: 401–404